MHD DARCY-FORCHHEIMER FLOW OF CHEMICALLY REACTING FLUIDS INROTATING FRAME WITH NON-LINEAR RADIATION AND ACTIVATION ENERGY

Poosappan Yesodha[1*], Kaliannan Saravanan[2]

Article History: Received: 12.12.2022 **Revised:** 29.01.2023 **Accepted:** 15.03.2023

Abstract

This research communication deliberates the Darcy-Forchheimer flow of chemically reacting fluids in rotating frame with magnetic field, activation energy and velocity slip condition. The energy expression is framed by nonlinear radiation and convective heating condition. The governing mathematical models are re-framed with the help of suitable variables and these resulting models are numerically computed by bvp4c algorithm in MATLAB. The physical interpretation of flow factors on velocities, temperature, concentration, skin friction coefficient, local Nusselt number and local Sherwood number are discussed through tables and diagrams. It is noted that the x_direction velocity decays and y_direction velocity improves when developing the magnetic field parameter. The Biot number and temperature ratio parameter develops the fluid temperature. The magnetic field and porosity parameter decays the skin friction coefficient. The thermal Biot number and radiation parameter improves the heat transfer rate. The mass Biot number and Schmidt number leads to strengthening the mass transfer rate.

KEYWORDS: Darcy-Forchheimer; MHD; Nonlinear thermal radiation; Activation energy; Chemical reaction; Convective heat/mass conditions.

[1]Department of Chemistry, Emerald Heights College for Women, Udhagamandalam, 643006 India

[2]Department of Chemistry, Thiruvalluvar Government Arts College, Rasipuram, 637401, India

Corresponding authors E-mail:*yesodhachemistry@gmail.com

1 Introduction

The transfer of heat and mass of a fluid

over a stretched surface has attracted many researchers due to its vast application in manufacturing processes in the industry. It finds importance in copper wire drawing, polymer extrusion, metallic plate rolling, paper production, cloth, glass fibre, plastic films where continuous stretching is required. The 3D unsteady flow of elastico-viscous fluid past a SS was investigated by Hayat et al. [1]. They clearly proved that $x-$ direction velocity improves and $y-$ direction velocity decays when escalating the values of stretching ratio parameter. Wang [2] examined the 3D flow through SS. The heat transmission analysis through SS was by Surma Devi et al. [3]. Hayat et al. [4] addressed the viscoelastic fluid flow through 3D SS. They proved that the SFC develops when improving the stretching ratio parameter. The 3D flow of viscous fluid with suction/injection was scrutinized by Lakshmisha et al. [5]. Bhuvaneswari et al. [6] developed the analytical and numerical solution of second-grade liquid flow past a SS with convective heating condition. They noted that the stretching ratio parameter decays the heat transfer gradient. The 3D radiative viscoelastic NF flow past a SS with Newtonian heating was inspected by Eswaramoorthi et al. [7]. They found that the NPVF decays on enriching stretching ratio parameter.

Many scientific and engineering endeavors rely heavily on the significance of flow via porous dispersion. In order to characterize the flow regime in a porous zone, it is common practice to use a dimensionless number (the Reynolds number). Darcy's law is useful to describe flow in

porous space at low flow rates. This law is inadequate when the Reynolds number exceeds one. Forchheimer [8] overcomes this restriction by incorporating a square component for velocity into the momentum equation. The momentousness of Darcy-Forchheimer flow of nanofluid past a SS with convective heating was addressed by Muhammad et al. [9]. They uncovered that the Forchheimer number leads to weaken the fluid velocity. Bakar et al. [10] deliberated the forced convective DFF flow over a shrinking sheet. They confirmed that the fluid velocity decays as improving the inertia-coefficient parameter in first solution and the opposite behavior attains in second solution. The heat transfer variations of DFF of nanofluids was numerically addressed by Umavathi et al. [11]. They undeniably proved that the Darcy number leads to improve the fluid temperature. Rasool et al. [12] evaluated the DFF of Jeffrey nanofluid past a SS with magnetic impact. They corroborated that the porosity factor expands the SBL. The 2D MHD DFF of Casson NF past an exponential sheet with stability analysis was examined by Lund et al. [13].

The effect of a magnetic field is especially helpful when making industrial equipment like pumps, MHD generators, metal casting, crystal growth, and so on. The 3D MHD DFF of Casson fluid in a rotating frame with CCHF theory was deliberated by Khan et al. [14]. They noticed that the larger quantity of magnetic field parameter intensifies the SFC for both directions. Veera Krishna et al. [15] deliberated the MHD time dependent flow of viscous fluid past a porous surface with magnetic impact. They noted that the fluid speed decays when improving the quantity of magnetic field parameter. Krishna and Chamkha [16] debriefed the MHD rotating flow past a porous medium. They detected that the magnetic field opposes the motion of the fluid and thinner the corresponding boundary layer. The MHD flow of viscous fluid past a vertical plate with Hall current was discussed by Sarma and Pandit [17]. Veera Krishna et al. [18] inspected the MHD radiative Casson hybrid nanofluid flow through a porous surface. They proved that the *Ag* nanofluid have lesser Shear stress when compared to the $Ag - TiO_2$ HNF when changing the magnetic field parameter. The heat transmission analysis of MHD viscous rotating fluid past a SS was presented by Rashad et al. [19]. He proved that the higher SFC occur in *x*-direction, whereas in the *y*-direction, the SFC to be lower. Nayak et al. [20] inspected the consequences of 3D MHD flow of micropolar Casson Cross NF. The magnetic field impact nanofluid flow past a rotating stretchable disk with convective boundary type constraints was studied by Mushtaq and Mustafa [21]. They noticed that the nanoparticle concentration improves when enriching the magnetic field parameter.

In many disciplines, including geothermal engineering, chemical engineering, oil emulsion, culinary arts, thermal insulation, food processing, mass commutation procedure attached by activation energy with chemical reaction is significant. Instead of experimental results, the theoretical results are needed to determine the flow effects of activation energy. Nevertheless, activation energy complicates the mass transport-chemical reaction relationship, therefore theoretical work on this area is scarce. The 3D rotating DFF of nanofluid past a SS with chemical reaction with Arrhenius activation energy was studied by Shafiq et al. [22]. They validated that the Arrhenius activation energy develops the heat flux. Rashid et al. [23] addressed the 3D DFF on a SS with AE. They authenticated that the fluid concentration is a suppressing function of reaction rate. The 3D rotating flow of NF past a sheet with AE was illustrated by Tayyab et al. [24]. They corroborated that the AE parameter develops the fluid concentration.

Based on the aforementioned studies, it has not yet been addressed how the magnetic field affects the rotation of the flow of thermally radiative viscous fluid past a heated surface with velocity slip. The primary purpose of this inquiry is to look at the impact that the phenomenon of

MHD rotative and DFF flow of thermally radiative viscous fluid with activation energy and binary chemical reaction. The governing mathematical models are re-framed into ODE models with the help of suitable conversions. These resultant ODE models are numerically computed by implementing the MATLAB bvp4c scheme.

2 Mathematical Formulation

Here we addressed the steady, 3D Darcy-Forchheimer flow in rotating frame subject to velocity slip. The energy model is framed through radiation. The consequences of activation energy and binary chemical reaction are added in our investigation. The flow that is induced by a stretched level surface corresponds with the plane that has $z \geq 0$. The fluid that is close to the wall has the velocity, temperature and concentration are (u_w, T_w, C_w) and larger than the free stream temperature and concentration are (T_∞, C_∞) respectively. The magnetic field of strength B_0 applied to the normal of sheet and the induced magnetic field is neglected due to small Reynolds number. The bottom of the sheet is heated through hot fluid with temperature T_f and this makes a heat transfer coefficient h_c. Under the above assumptions, the governing flow models are expressed as follows:

$$\frac{\partial u}{\partial x}+\frac{\partial v}{\partial y}+\frac{\partial w}{\partial z}=0 \tag{1}$$

$$u\frac{\partial u}{\partial x}+v\frac{\partial u}{\partial y}+w\frac{\partial u}{\partial z}-2\Omega v=\nu\frac{\partial^2 u}{\partial z^2}-\frac{\nu}{k_1}u-Fu^2-\frac{\sigma B_0^2}{\rho}u \tag{2}$$

$$u\frac{\partial v}{\partial x}+v\frac{\partial v}{\partial y}+w\frac{\partial v}{\partial z}+2\Omega u=\nu\frac{\partial^2 v}{\partial z^2}-\frac{\nu}{k_1}v-F\nu^2-\frac{\sigma B_0^2}{\rho}v \tag{3}$$

$$u\frac{\partial T}{\partial x}+v\frac{\partial T}{\partial y}+w\frac{\partial T}{\partial z}=\alpha\frac{\partial^2 T}{\partial z^2}+\frac{1}{\rho c_p}\frac{16\sigma^*}{3k^*}\frac{\partial}{\partial z}\left(T^3\frac{\partial T}{\partial z}\right) \tag{4}$$

$$u\frac{\partial C}{\partial x}+v\frac{\partial C}{\partial y}+w\frac{\partial C}{\partial z}=D\frac{\partial^2 C}{\partial z^2}-k_r^2\left(\frac{T}{T_\infty}\right)^n e^{\frac{-E_a}{kT}}(C-C_\infty) \tag{5}$$

Here (u, v, w)-velocity factors along the (x, y, z) directions, Ω-angular velocity, ν-kinematic viscosity, k_1-porous medium permeability, σ-electrical conductivity of the fluid, B_0-applied magnetic field, ρ-density of the fluid, α-thermal diffusivity, c_p is the specific heat, k_T -thermal conductivity, k_r^2-chemical reaction rate constant, n-exponent fitted rate, σ^*-Stefan-Boltzmann constant. The corresponding boundary conditions:

$$u=ax+L\frac{\partial u}{\partial z},\quad v=0,\ w=0,-k\frac{\partial T}{\partial z}=h_T(T_w-T),\ -D\frac{\partial C}{\partial z}=h_C(C_w-C),\text{ when z = 0}$$

$$u\to 0,\ v\to 0,\ T\to T_\infty,\ C\to C_\infty\ as\ z\to\infty \tag{6}$$

Define

$$u=axf'(\eta),\quad v=axg(\eta),\quad w=-\sqrt{a\nu}\,f(\eta),\ \eta=z\sqrt{\frac{a}{\nu}},$$

$$\theta(\eta)=\frac{T-T_\infty}{T_w-T_\infty},\qquad \phi(\eta)=\frac{C-C_\infty}{C_w-C_\infty}, \tag{7}$$

Applying equation (7) in equations (2-5), we have

$$f'''(\eta)+f(\eta)f''(\eta)-\lambda f'(\eta)+2\beta g(\eta)-(1+F_r)f'(\eta)-Mf'(\eta)=0 \tag{8}$$

$$g''(\eta)+f(\eta)g'(\eta)-f'(\eta)g(\eta)-2\beta f'(\eta)-\lambda g(\eta)-F_r g(\eta)g(\eta)-Mg(\eta)=0 \tag{9}$$

$$\left(\frac{1}{Pr}\right)\theta''(\eta)+f(\eta)\theta'(\eta)+\frac{1}{Pr}\frac{4}{3}Rd\begin{bmatrix}(\theta_w-1)^3\{3\theta^2(\eta)\theta'^2(\eta)+\theta^3(\eta)\theta''(\eta)\}+\\(\theta_w-1)^2\{6\theta(\eta)\theta'^2(\eta)+3\theta^2(\eta)\theta''(\eta)\}+\\(\theta_w-1)\{3\theta'^2(\eta)+3\theta(\eta)\theta''(\eta)\}+\theta''(\eta)\end{bmatrix}=0 \tag{10}$$

$$\phi''(\eta)+Scf(\eta)\phi'(\eta)-Sc\,\sigma\,[1+\delta\theta(\eta)]^n\exp\left[-\frac{E}{1+\delta\theta(\eta)}\right]\phi=0 \tag{11}$$

Here λ-porosity parameter, β-rotational parameter, *Fr*-Forchheimer number, *M* -magnetic field parameter, *Pr*-Prandtl number, *Sc*-Schmidt number, *d*-slip parameter, *E*-activation energy parameter, δ-temperature difference parameter, θ_w-temperature ratio parameter, *Rd*-radiation parameter, σ^{**}-reaction rate, Bi_T & Bi_C-temperature and mass Biot number.
The appropriate boundary conditions (6) are remodeled as follows,

$$f(0) = 0,\ f'(0) = 1 + df''(0),\ \mathrm{g}(0) = 0,\ \ \theta' = -Bi_T(1-\theta),\ \ \phi' = -Bi_C(1-\phi)$$
$$f'(\infty) \to 0, \mathrm{g}(\infty) \to 0, \theta(\infty) \to 0, \phi(\infty) \to 0 \text{ as } \eta \to 0 \qquad (12)$$

The unit-less form of skin friction coefficient, local Nusselt and Sherwood numbers are expressed as follows:

$$C_{fx}\sqrt{Re_x} = f''(0);\ \frac{Nu_x}{\sqrt{Re_x}} = \left[1 + \frac{4}{3}R\{1 + (\theta_w - 1)\theta(0)\}^3\right]\theta'(0);\ \ \frac{Sh_x}{\sqrt{Re_x}} = -\phi'(0),$$

where Re_x is the local Reynolds number.

2.1 Numerical Solutions

The reduced ODE models 8-11 are solved numerically by applying the MATLAB bvp4c algorithm. In this regard, initially we convert the higher order equations to first order equations. Let us take $f = H_1$, $f' = H_2$, $f'' = H_3$, $g = H_4$, $g' = H_5$, $\theta = H_6$, $\theta' = H_7$, $\varphi = H_8$, $\varphi' = H_9$
The first order system of equations are

$$\begin{aligned}
H_1' &= H_2\\
H_2' &= H_3\\
H_3' &= -H_1H_3 + (\lambda + M)H_2 - 2\beta H_4 + (1+Fr)H_2^2\\
H_4' &= H_5\\
H_5' &= -H_1H_5 + H_2H_4 + (\lambda + M)H_4 + 2\beta H_2 + FrH_4^2\\
H_6' &= H_6\\
H_7' &= \frac{D_1}{D_2}\\
H_8' &= H_8\\
H_9' &= -ScH_1H_9 + Sc\sigma[1+\delta H_6]^n Exp\left[-\frac{E}{1+\delta H_6}\right]H_8
\end{aligned}$$

where

$$D_1 = -H_1H_7 - \frac{1}{Pr}\frac{4}{3}Rd[3(\Lambda-1)^3H_6^2H_7^2 + 6(\Lambda-1)^2H_6H_7^2 + 3(\Lambda-1)H_7^2]$$
$$D_2 = \frac{1}{Pr} + \frac{1}{Pr}\frac{4}{3}Rd[(\Lambda-1)^3H_6^3 + 3(\Lambda-1)^2H_6^2 + 3(\Lambda-1)H_6 + 1]$$

With the corresponding conditions

$$\begin{aligned}
&H_1(0) = 0,\ H_2(0) = 1 + dH_3(0),\ \ H_2(\infty) \to 0,\\
&H_4(0) = 0,\ H_4(\infty) \to 0,\\
&H_7 = -Bi_T(1-H_6),\ \ H_6(\infty) \to 0,\\
&H_9 = -Bi_C(1-H_8),\ \ H_8(\infty) \to 0
\end{aligned} \qquad (13)$$

3 Result and Discussion

This section seeks to examine the impacts of different physical elements on the velocity profile $f'(\eta)$, transverse velocity profile $g(\eta)$, temperature profile $\theta(\eta)$ and concentration profile $\varphi(\eta)$. Table 1 elucidates the comparison of $f''(0)$ and $g'(0)$ for different extent of G with Najwa Maqsood et al. [25]. It is noted that there is an outstanding achievement with the earlier publication. The values of $f''(0)$ and $g'(0)$ for different extent of M, λ, Fr and G with d=0.0 and d=0.6 are shown in Table 2. From this table it is invented that the velocity profile slows when enhancing the extent of M, λ, Fr and G whereas the transverse velocity profile enhances when heightening the values of M, λ, Fr and it declines when enhancing the extent of G. Table 3 provides the extent of $\frac{Nu}{\sqrt{Re}}$ and $\frac{Sh}{\sqrt{Re}}$ for disparate extent of M, λ, Fr, G, Rd and Bi_T with $\theta_w = 1$ and $\theta_w = 1.3$. It is observed that the Nusselt number and Shearwood number declines when raising the extent of M, λ, Fr and G, whereas it raises when raising the values of Rd and Bi_T. The extent of $\frac{Sh}{\sqrt{Re}}$ for different extent of σ, n, E, δ and Bi_C with d=0.0 and d=0.6 are described in Table 4. It is seen that the Shearwood number enhances for enhancing the extent of σ, n, δ and Bi_C whereas it declines when enhancing the extent of E.

Figure 1(a-d) reveals the influence of velocity profile against M, λ, Fr and G with d=0.0 and d=0.6. It is found that the velocity profile decays as the extent of M, λ, Fr and G increases. The influence of transverse velocity profile against M, λ, Fr and G with d=0.0 and d=0.6 are examined in Figure 2(a-d). It is seen that the transverse velocity profile enlarges when enlarging the quantity of M, λ and Fr and it decays when enhancing the quantity of G. Physically, the velocity profile is devalued while the temperature profile is elevated when the magneticfield parameter increases. This is because an increase in the value of the parameter characterising the magnetic field generates an opposing force to the flow, known as the Lorentz force. This force has tendency to lessen the velocity boundary layer and heightens the thermal boundary layer thickness. Figure 3(a-d) exposed the influence of temperature profile against Rd, θ_w, Bi_T and G with d=0.0 and d=0.6. It is intensified that the temperature profile strengthens when elevating the extent of Rd, θ_w, Bi_T and G. Physically, the higher the Biot number, the greater the heat transfer coefficient, which in turn raises the fluid temperature and expands the thermalboundary layer.

The effectuates of σ, E, n, δ on the concentration profile are delineated in Figure 4(a-d). It has been noted that the concentration profile decays when strengthening the extent of σ, δ and n and it enhances when heightening the value of E. Figure 5(a-b) portrays the concentration profile against G and Bi_C. It is observed that the concentration profile upsurges when upsurging the extent of G and Bi_C. Physically, a more accurate estimation of the variation in the chemical reaction leads to a thickening of the solutal layer. Hence, the concentration profile gradually decreases. The changes of SFC for disparate extent of M, λ and G with d=0.0 and d=0.6 are shown in Figure 6(a-b). It is seen that the surface drag force slumps when declining the values of M and G. Physically, Lorentz force theory suggests that a drag type force plays a significant part in maintaining the fluid's velocity. Hence, the SFC decreases as the magnetic field parameter is increased. Figure 7(a-b) displays that the LNN for different extent of Rd, Bi_T and θ_w with d=0.0 and d=0.6. It is noted that the LNN grows as the Rd, Bi_T and θ_w increases. Physically, by augmenting the rate of energy transfer to the fluid, augmenting the radiation parameter enhances the LNN and expands the surface velocity. The LSN for various extent of E, Sc and Bi_C are displayed in Figure 8(a-b). It is found that the LSN decays when enhancing the value of E

and Bi_C and the opposite trend is obtained for Sc and Bi_C. Physically, improve in values of activation energy lower the Sherwood number.

3 Conclusions

This study report covers topics such as the Darcy-Forchheimer flow of chemically reacting fluids in a rotating frame with magnetic field, activation energy, and velocity slip condition. As a framework for the depiction of energy, the condition of nonlinear radiation and convective heating acts as a necessary prerequisite. The mathematical models that are used to manage the situation are re-framed with the help of variables that are suitable, and the bvp4c technique in MATLAB is used to execute numerical calculations on the re-framed models.

The investigation's results back up the hypotheses given below.

- The both velocity fields are decayed in opposition to higher rotational parameter.
- The radiation parameter and Biot makes a considerable contribution to the fluid temperatures improvement.
- The activation energy and temperature difference parameters contributes to develop thefluid concentration.
- The heat transfer gradient is high in non-linear radiation cases than the linear radiationcases
- The mass Biot number and temperature difference parameter develops the mass transfergradient.

Table 1: The comparison of $f''(0)$ and $g'(0)$ for different values of G with Najwa Maqsood et al. [25].

G	$f''(0)$		$g'(0)$	
	Present Result	Ref. [25]	Present Result	Ref. [25]
0	−1.00000	−1.000000	0.000000	0.000000
0.2	−1.03310	−1.033105	−0.238546	−0.238456
0.4	−1.10091	−1.100905	−0.430962	−0.430962
0.5	−1.13838	−1.138381	−0.512760	−0.512760
0.6	−1.17636	−1.176365	−0.587418	−0.587418
0.8	−1.25178	−1.251776	−0.720361	−0.720361
1.0	−1.32503	−1.325029	−0.837099	−0.837098
1.2	−1.39560	−1.395596	−0.941998	−0.941998
1.4	−1.46345	−1.463452	−1.037842	−1.037841
1.6	−1.52874	−1.528736	−1.126507	−1.126507
1.8	−1.59164	−1.591637	−1.209321	−1.209321
2	−1.65235	−1.652352	−1.287259	−1.287258
3	−1.92893	−1.928932	−1.624735	−1.624735
4	−2.17159	−2.171594	−1.905393	−1.905391
5	−2.39014	−2.390142	−2.150526	−2.150523

Table 2: The value of $f''(0)$ and $g'(0)$ for different values of M, λ, Fr and G with d=0.0 and d=0.6.

M	λ	Fr	G	d=0		d=0.6	
				$f''(0)$	$g'(0)$	$f''(0)$	$g'(0)$
0	0.2	0.4	0.5	−1.30551	−0.470412	−0.66904	−0.313160
0.5				−1.46022	−0.398967	−0.72134	−0.248264
1				−1.60987	−0.350088	−0.76815	−0.204474
1.5				−1.75115	−0.314872	−0.80870	−0.173851
2				−1.88404	−0.288209	−0.84377	−0.151424
0.5	0	0.4	0.5	−1.39854	−0.424187	−0.70092	−0.271164
	0.4			−1.52100	−0.377309	−0.74083	−0.228726
	0.8			−1.63882	−0.342159	−0.77675	−0.197495
	1.2			−1.75115	−0.314872	−0.80870	−0.173851
	1.6			−1.85810	−0.293018	−0.83715	−0.155412
0.5	0.2	0	0.5	−1.36967	−0.404177	−0.70354	−0.254741
		0.6		−1.50364	−0.396567	−0.72956	−0.245289
		1.2		−1.62750	−0.390068	−0.75202	−0.237237
		1.8		−1.74320	−0.384466	−0.77176	−0.230255
		2.4		−1.85211	−0.379613	−0.78935	−0.224117
0.5	0.2	0.4	0	−1.40001	0.000000	−0.69684	0.000000
			1	−1.58272	−0.716053	−0.76437	−0.415302
			2	−1.84687	−1.180799	−0.84114	−0.611989
			3	−2.09137	−1.531140	−0.89993	−0.728969
			4	−2.31390	−1.821265	−0.94609	−0.809651

Table 3: The value of $\frac{Nu}{\sqrt{Re}}$ and $\frac{Sh}{\sqrt{Re}}$ for different values of M, λ, Fr, G, Rd and $\mathrm{Bi_T}$ with $\theta_\mathrm{W} = 1$ and $\theta_\mathrm{W} = 1.3$.

M	λ	Fr	G	Rd	$\mathrm{Bi_T}$	$\theta_\mathrm{W} = 1$		$\theta_\mathrm{W} = 1.3$	
						$\frac{Nu}{\sqrt{Re}}$	$\frac{Sh}{\sqrt{Re}}$	$\frac{Nu}{\sqrt{Re}}$	$\frac{Sh}{\sqrt{Re}}$
0	0.2	0.4	0.5	0.6	0.4	0.35114	0.256798	0.39890	0.257359
0.5						0.33816	0.255364	0.38425	0.255968
1						0.32206	0.254047	0.36548	0.254706
1.5						0.30579	0.252953	0.34625	0.253663
2						0.29043	0.252066	0.32796	0.252818
0.5	0	0.4	0.5	0.6	0.4	0.34400	0.255939	0.39095	0.256522
	0.4					0.33186	0.254813	0.37696	0.255439
	0.8					0.31877	0.253810	0.36161	0.25448
	1.2					0.30579	0.252953	0.34625	0.253663
	1.6					0.29341	0.252229	0.33151	0.252973
		0	0.5	0.6	0.4	0.34331	0.255824	0.39023	0.256410
0.5	0.2	0.6				0.33572	0.255154	0.38141	0.255767
		1.2				0.32888	0.254589	0.37342	0.255226
		1.8				0.32262	0.254104	0.36608	0.254762
		2.4				0.31687	0.253681	0.35930	0.254357
0.5	0.2	0.4	0	0.6	0.4	0.35884	0.256650	0.40903	0.257166
			1			0.30120	0.253522	0.33940	0.254259
			2			0.24172	0.251101	0.26827	0.251942
			3			0.20490	0.249694	0.22624	0.250515
			4			0.18125	0.248765	0.20035	0.249535
0.5	0.2	0.4	0.5	0	0.4	0.23351	0.253916	0.23351	0.253916
				2		0.48044	0.257146	0.57023	0.258172
				4		0.61062	0.258185	0.73828	0.259097
				6		0.72643	0.258642	0.90602	0.259414
				8		0.84096	0.258890	1.07918	0.259566
0.5	0.2	0.4	0.5	0.6	0	0	0.250602	0	0.250602
					2	0.54169	0.257804	0.59613	0.258468
					4	0.58576	0.258298	0.63480	0.258896
					6	0.60209	0.258478	0.64845	0.259045
					8	0.61060	0.258571	0.65541	0.259120

Table 4: The value of $\frac{Sh}{\sqrt{Re}}$ for different values of σ, n, E, δ and Bi_C with d=0 and d=0.6.

σ	n	E	δ	Bi_C	$\frac{Sh}{\sqrt{Re}}$	
					d=0	d=0.6
0	0.5	0.3	0.5	0.4	0.21867	0.17925
1					0.29189	0.28810
2					0.31271	0.31128
3					0.32426	0.32363
4					0.33196	0.33170
0.4	0	0.3	0.5	0.4	0.26329	0.25245
	2				0.27203	0.26713
	4				0.28203	0.28310
	6				0.29309	0.29957
	8				0.30487	0.31565
0.4	0.5	0	0.5	0.4	0.27238	0.26442
		0.5			0.26088	0.25041
		1			0.25066	0.23697
		1.5			0.24206	0.22458
		2			0.23523	0.21367
0.4	0.5	0.3	0	0.4	0.26219	0.25060
			2		0.27250	0.26689
			4		0.27903	0.27581
			6		0.28377	0.28185
			8		0.28749	0.28638
0.4	0.5	0.3	0.5	0	0	0
				0.5	0.30594	0.29354
				1	0.44080	0.41550
				1.5	0.51673	0.48230
				2	0.56542	0.52446

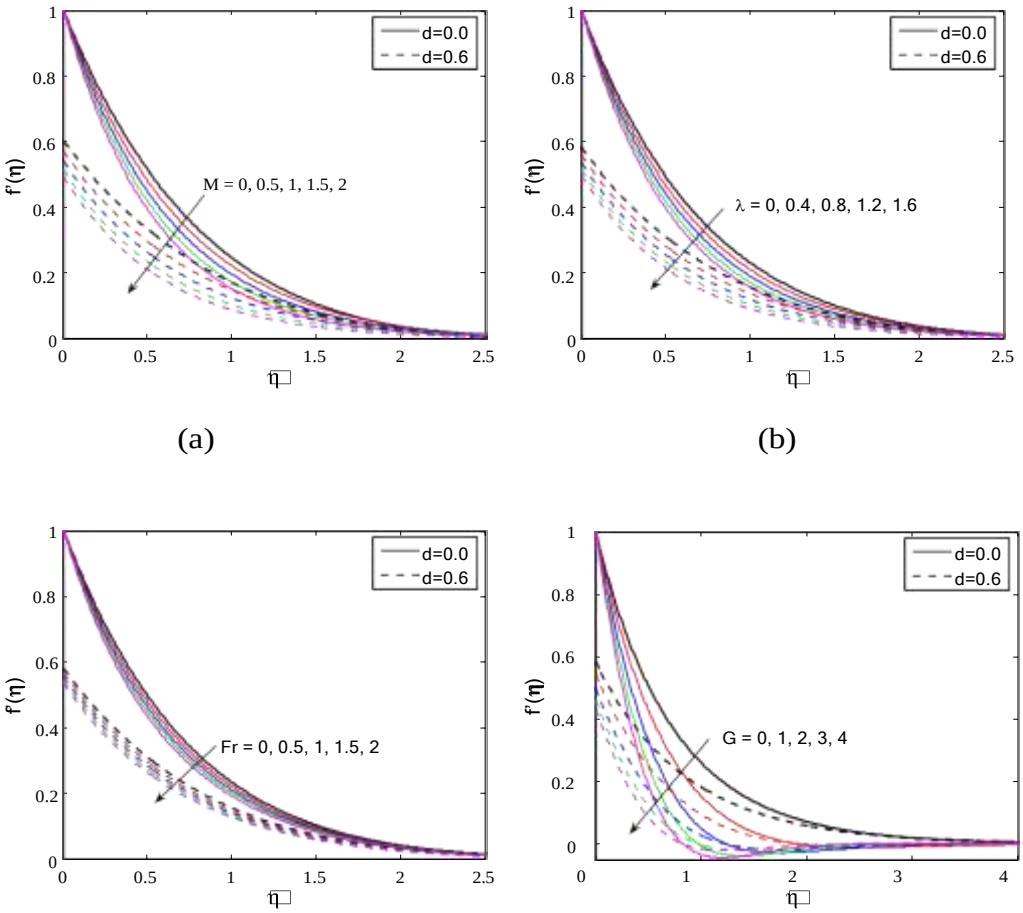

Figure 1: The velocity profile against M(a), λ(b), Fr(c) and G(d) with d=0 and d=0.6.

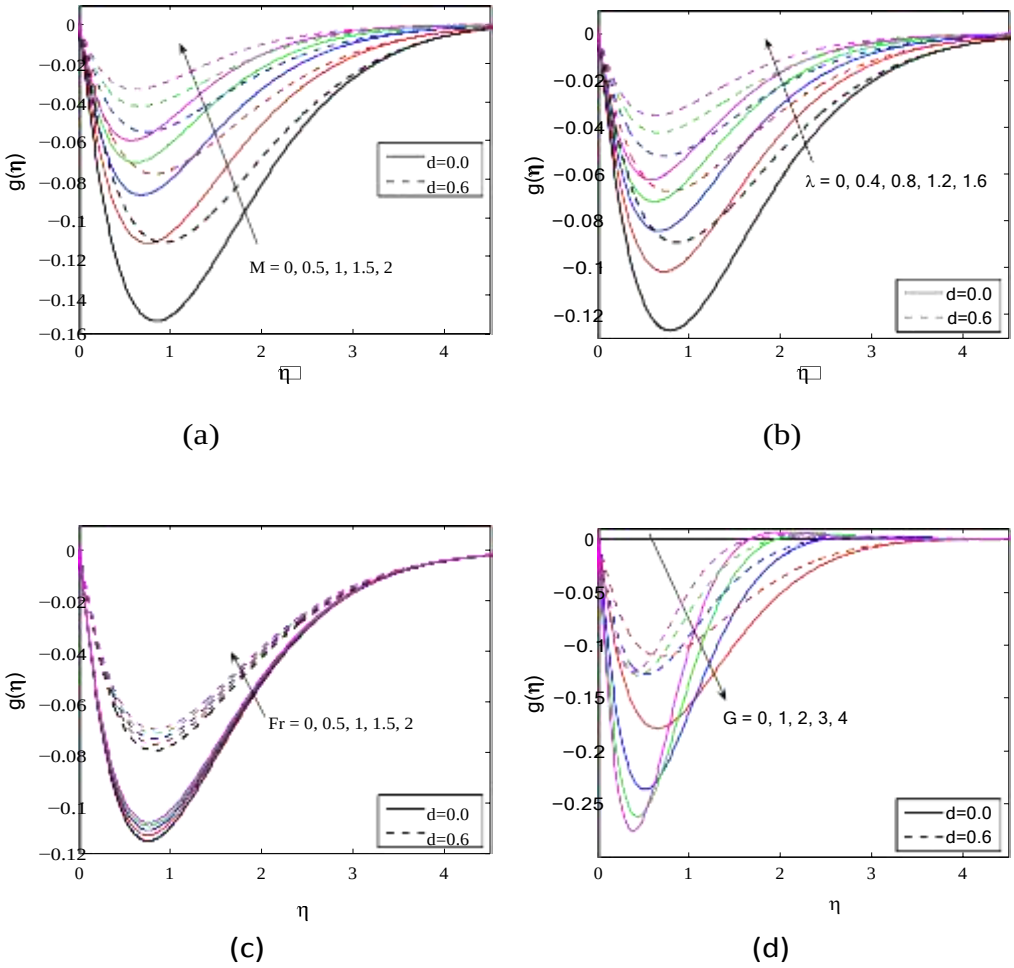

Figure 2: The velocity profile against M(a), λ(b), Fr(c) and G(d) with d=0 and d=0.6.

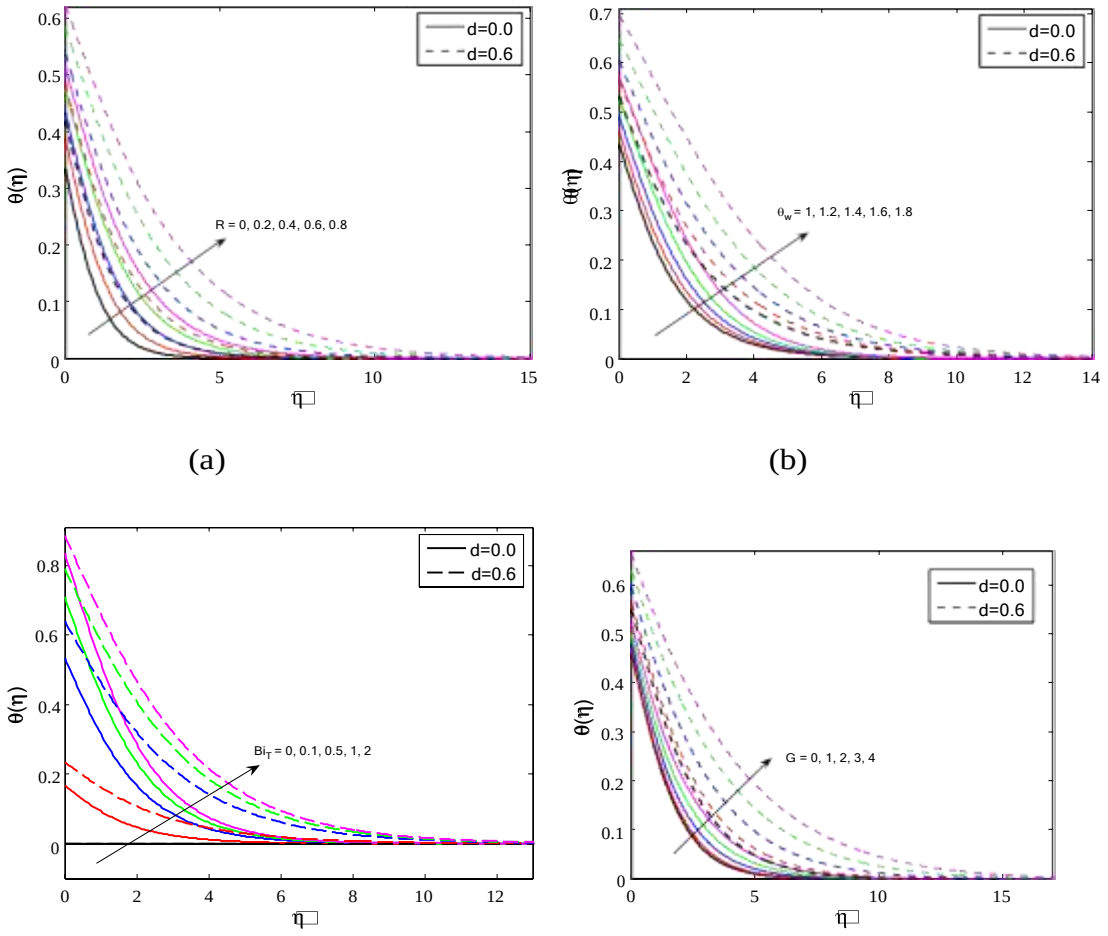

Figure 3: The temperature profile against R(a), θ_w(b), Bi_T(c) and G(d) with d=0 and d=0.6.

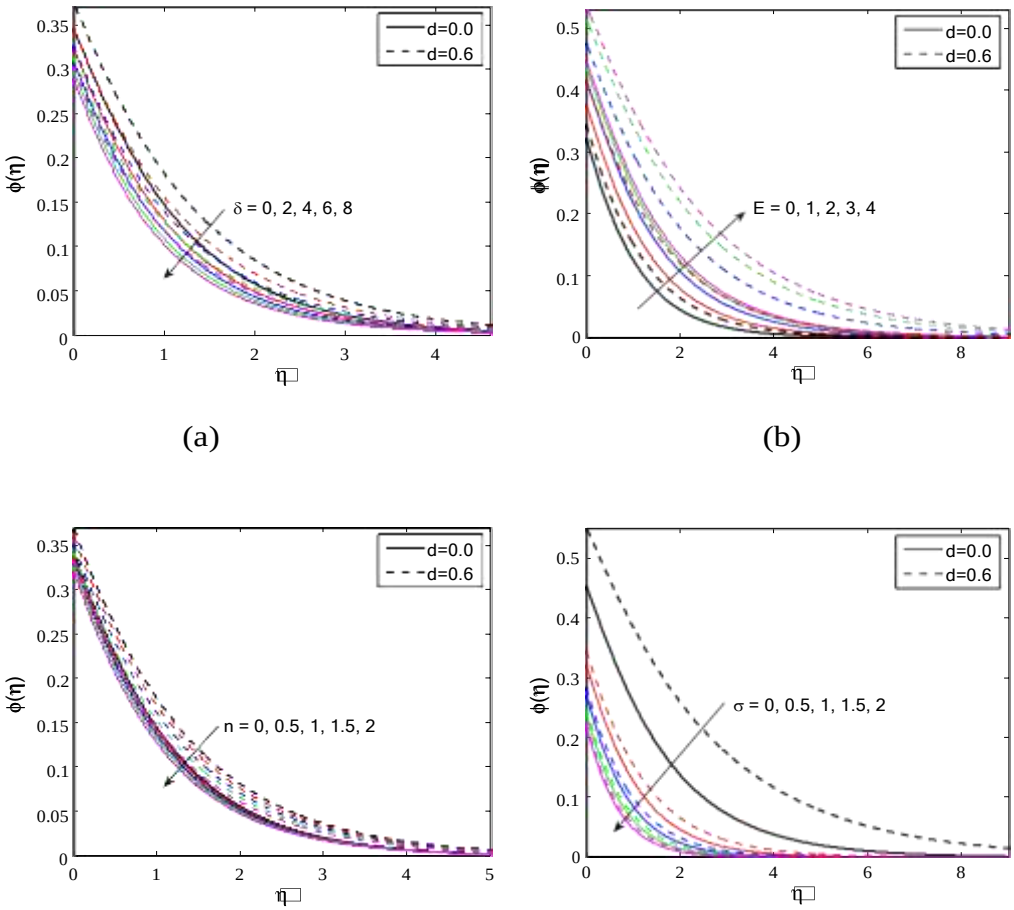

Figure 4: The concentration profile against δ(a), E(b), n(c) and σ(d) with d=0 and d=0.6.

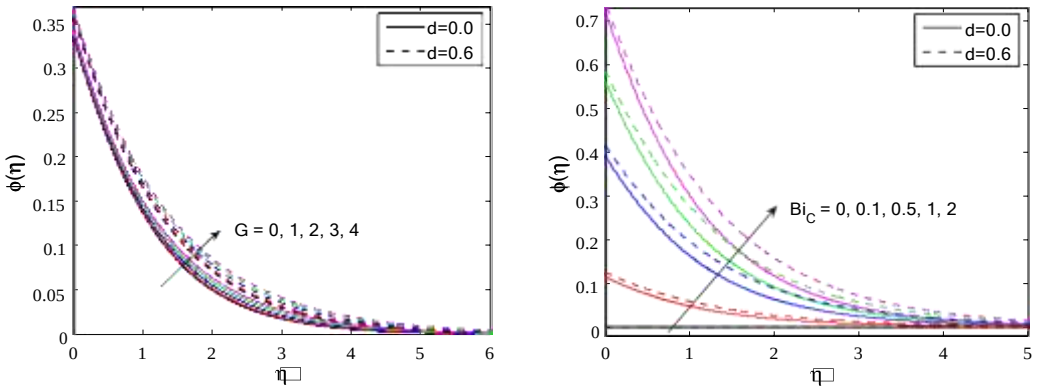

(a) (b)

Figure 5: The concentration profile against G(a) andBi_C(b) with d=0 and d=0.6.

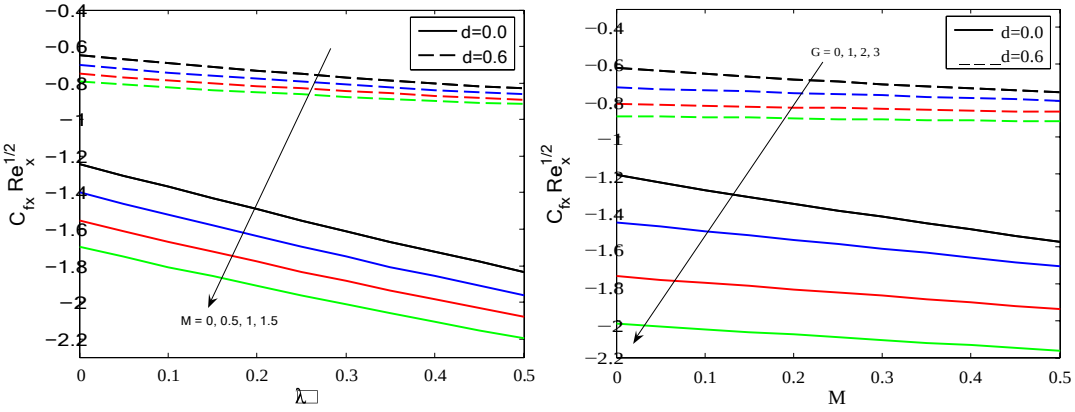

(a) (b)

Figure 6: The SFC for different combinations of M, λ and G with d=0 and d=0.6.

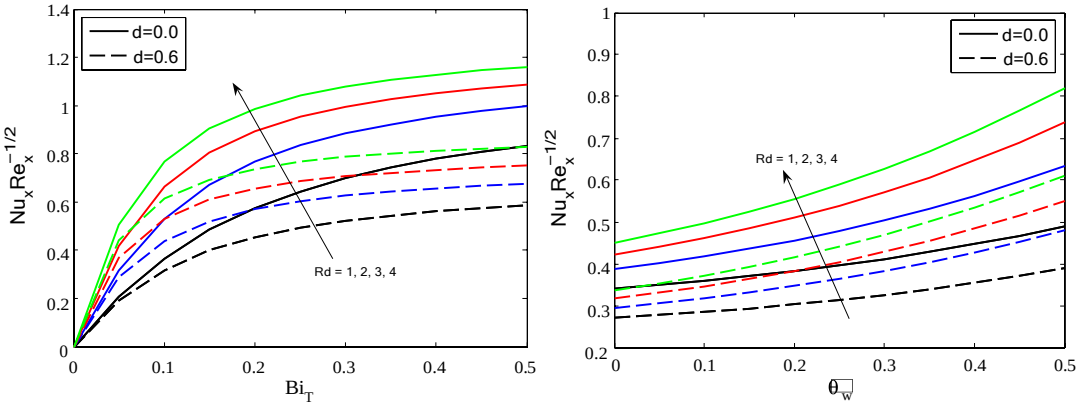

(a) (b)

Figure 7: The LNN for different combinations of Rd, Bi_T and θ_w with d=0 and d=0.6.

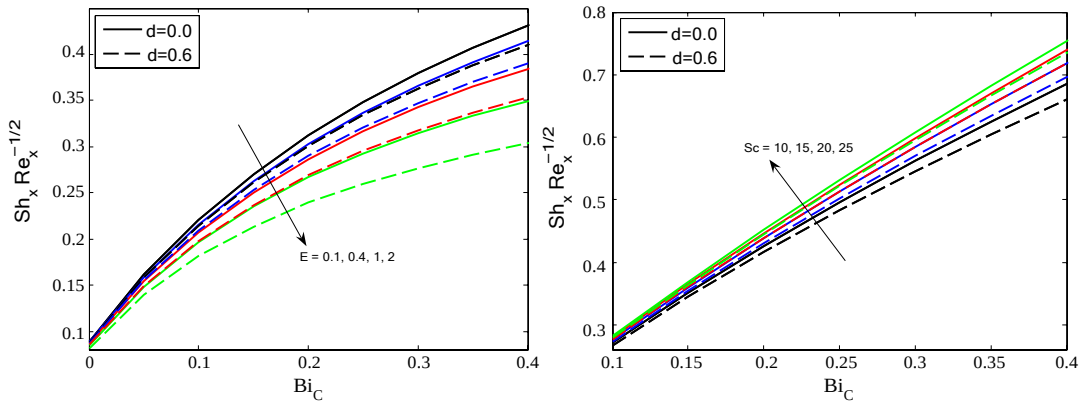

(a) (b)

Figure 8: The LSN for different combinations of E, Bi_C and Sc with d=0 and d=0.6.

References

[1] Hayat, T., Mustafa, M. and Hendi, A.A. Time dependent three-dimensional flow and mass transfer of elastico-viscous fluid over unsteady stretching sheet, Appl. Math. Mech., (English Ed.) 32(2), pp. 167-178, 2011.

[2] Wang C Y, The three-dimensional flow due to a stretching flat surface, Phys. Fluids 27 pp1915-1917, 1984.

[3] Surma Devi C D, Takhar HS and Nath G, Unsteady three dimensional boundary layer flow due to a stretching surface Int. J. Heat Mass Transf. 29 pp 1996-1999, 1986.

[4] T. Hayat, M. Sajid, I. Pop, Three-dimensional flow over a stretching surface in a viscoelastic fluid, Nonlinear Analysis: Real World Applications 9 (2008) 1811-1822.

[5] Lakshmisha K N, Venkateshwaran S and Nath G, Three dimensional unsteady flow with heat and mass transfer over a continuous stretching surface, J. Heat Transf. 115 pp 590-595,1988.

[6] M. Bhuvaneswari, S. Eswaramoorthi, S. Sivasankarana, S. Rajan, and A. Saleh Alshomrani, Effects of viscous dissipation and convective heating on convection flow of a second-grade liquid over a stretching surface: An analytical and numerical study, Scientia Iranica B (2019) 26(3), 1350-1357.

[7] S. Eswaramoorthi, M. Bhuvaneswari, S. Sivasankaran and H. Niranjan, Thermally radiative flow of a viscoelastic nanofluid with Newtonian heating, Int. J. Nanotechnol., Vol. 18, Nos. 5/6/7/8, 2021, 14 pages.

[8] P. Forchheimer, "Wasserbewegung durch boden," Zeitschrift des Vereins deutscher Inge- nieure, vol. 45, pp. 1782-1788, 1901.

[9] T. Muhammad, D.-C. Lu, B. Mahanthesh, M.R. Eid, M. Ramzan, A. Dar, Significance of Darcy-Forchheimer porous medium in nanofluid through carbon nanotubes, Commun. Theor. Phys. 70 (2018) 361-366.

[10] S.A. Bakar, N.M. Arifin, R. Nazar, F.Md. Ali, I. Pop, Forced convection boundary layer stagnation-point flow in Darcy-Forchheimer porous medium past a shrinking sheet, Front. Heat Mass Transf. 7 (2016) 7 pages.

[11] J.C. Umavathi, O. Ojjela and K. Vajravelu, "Numerical analysis of natural convective flow and heat transfer of nanofluids in a vertical rectangular duct using Darcy-Forchheimer- Brinkman model," *International Journal of Thermal Sciences*, vol. 111, pp. 511-524, (2017).

[12] Rasool, G.; Shafiq, A.; Durur, H. Darcy-Forchheimer relation in Magnetohydrodynamic Jeffrey nanofluid flow over stretching surface. Discret. Contin. Dyn. Syst. Ser. S 2019.

[13] Lund, L.A.; Omar, Z.; Khan, I.; Raza, J.; Bakouri, M.; Tlili, I. Stability analysis of Darcy-Forchheimer flow of Casson type nanofluid over an exponential sheet: Investigation of critical points. Symmetry 2019, 11, 412.

[14] M. N. Khan, A. Ahmed, N. A. Ahammad, T. Alqahtani, S. Algarni, Insights into 3D flow of Casson fluid on exponential stretchable surface in rotating frame through porous medium, Ain Shams Engineering Journal 14 (2023) 101849, 10 pages.

[15] M. Veera Krishna, N. Ameer Ahamad, Ali J. Chamkha, Numerical investigation on unsteady MHD convective rotating flow past an infinite vertical moving porous surface, Ain Shams Engineering Journal 12 (2021) 2099-2109.

[16] Krishna MV, Chamkha AJ. Hall and ion slip effects on MHD rotating flow of elastico viscous fluid through porous medium. Int Commun Heat Mass Transfer 2020;113:.

[17] Sarma D, Pandit KK. Effects of Hall current, rotation and Soret effects on MHD free convection heat and mass transfer flow past an accelerated vertical plate through a porous medium. Ain Shams Eng J 2018;9:631-46.

[18] M. Veera Krishna, N. Ameer Ahammad, Ali J. Chamkha, Radiative MHD flow of Casson hybrid nanofluid over an infinite exponentially accelerated vertical porous surface, Case Studies in Thermal Engineering 27 (2021) 101229, 15 pages.

[19] A.M. Rashad, Effects of radiation and variable viscosity on unsteady MHD flow of a rotating fluid from stretching surface in porous medium, Journal of the Egyptian Mathematical Society (2014) 22, 134-142.

[20] M.K. Nayak, A.K.A. Hakeem, B. Ganga, M.I. Khan, M. Waqas, O.D. Makinde, Entropy optimized MHD 3D nanomaterial of non-Newtonian fluid: a combined approach to good absorber of solar energy and intensification of heat transport, Comput. Methods Progr. Biomed. 186 (2020), 105131.

[21] A. Mushtaq, M. Mustafa, Computations for nanofluid flow near a stretchable rotating disk with axial magnetic field and convective conditions, Results in Physics 7 (2017) 3137-3144.

[22] A. Shafiq, G. Rasool, C.M. Khalique, "Significance of thermal slip and convective boundary conditions in three dimensional rotating Darcy-Forchheimer nanofluid flow," *Symmetry*, vol. 12, no. 5, 21 pages, (2020).

[23] Rashid, S.; Hayat, T.; Qayyum, S.; Ayub, M.; Alsaedi, A. Three dimensional rotating Darcy-Forchheimer flow with activation energy. Int. J. Numer. Methods Heat Fluid Flow,2019.

[24] M. Tayyab, I. Siddique, F. Jarad, M.K. Ashraf, B. Ali, "Numerical solution of 3D rotating nanofluid flow subject to Darcy-Forchheimer law, bio-convection and activation energy," *South African Journal of Chemical Engineering*, vol. 40, pp. 48-56, (2022).

[25] Najwa Maqsood, M. Mustafa, Junaid Ahmad Khan, Numerical tackling for viscoelastic fluid flow in rotating frame considering homogeneous-heterogeneous reactions, *Results in Physics*, 7, pp. 3475-3481 (2017).